RESEARCH ARTICLE

Energy & Environmental Materials WILEY

Electronic Textiles

Sustainable, Wearable, and Eco-Friendly Electronic Textiles

Marzia Dulal, Harsh Rajesh Mansukhlal Modha, Jingqi Liu, Md Rashedul Islam, Chris Carr, Tawfique Hasan, Robin Michael Statham Thorn, Shaila Afroj, and Nazmul Karim**

Wearable electronic textiles (e-textiles) with embedded electronics offer promising solutions for unobtrusive, real-time health monitoring, enhancing healthcare efficiency. However, their adoption is limited by performance and sustainability challenges in materials, manufacturing, and recycling. This study introduces a sustainable paradigm for the fabrication of fully inkjet-printed Smart, Wearable, and Eco-friendly Electronic Textiles (SWEET) with the first comprehensive assessments of the biodegradability and life cycle assessment (LCA). SWEET addresses existing limitations, enabling concurrent and continuous monitoring of human physiology, including skin surface temperature (at temperature coefficient of resistance, TCR value of ∼−4.4% °C^{-1}) and heart rate (∼74 beats per minute, bpm) separately and simultaneously like the industry gold standard, using consistent, versatile, and highly efficient inkjet-printed graphene and Poly (3,4-ethylenedioxythiophene): poly (styrene sulfonate) (PEDOT: PSS)-based wearable e-textiles. Demonstrations with a wearable garment on five human participants confirm the system's capability to monitor their electrocardiogram (ECG) signals and skin temperature. Such sustainable and biodegradable e-textiles decompose by ∼48% in weight and lost ∼98% strength over 4 months. Life cycle assessment (LCA) reveals that the graphene-based electrode has the lowest climate change impact of ∼0.037 kg CO_2 eq, 40 times lower than reference electrodes. This approach addresses material and manufacturing challenges, while aligning with environmental responsibility, marking a significant leap forward in sustainable e-textile technology for personalized healthcare management.

1. Introduction

Textile, often referred to as the "second skin" of the human body, has a history dating back as far as ∼27 000 years. However, textiles, a key part of modern civilization, is considered to be the second-most polluting industry after the oil sector,[1] producing ∼92 million tons of textile waste annually.[2] Although, ∼95% of textiles are fully recyclable, ∼85% find their way to landfills.[3] In recent years, multifunctional wearable e-textiles capable of identifying and differentiating various stimuli, along with the capacity to gather and store a diverse array of signals using a single device, have held considerable significance for personalized healthcare applications.[4] However, the integration of electronics into conventional textiles to create wearable e-textiles further complicates the end-of-life processing of such electronic waste (e-waste), because they often contain non-textile components like electronics and interconnections, making disassembly challenging or even impractical.[5]

The rapid aging of the world population, with an estimated ∼22% expected to be aged over 60 by 2050 poses substantial future challenges to the global healthcare system. Since a significant portion (∼80%) of the elderly population will reside in low- and middle-income countries, the burden on healthcare systems is likely to intensify. The increased prevalence of age-related health issues, coupled with a

M. Dulal, Dr. M. R. Islam, Dr. S. Afroj, Prof. N. Karim
Centre for Print Research (CFPR), The University of the West of England, Bristol BS16 1QY, UK
E-mail: s.afroj@exeter.ac.uk
E-mail: nazmul.karim@soton.ac.uk
H. R. M. Modha, Dr. R. M. S. Thorn
Centre for Sustainable Agri-Food and Environment, School of Applied Sciences, University of the West of England, Bristol BS16 1QY, UK
Dr. J. Liu
Department of Mechanical Engineering, University of Bath, Bath BA2 7AY, UK
Prof. C. Carr
Clothworkers' Centre for Textile Materials Innovation for Healthcare, School of Design, University of Leeds, Leeds LS2 9JT, UK
Prof. T. Hasan
Cambridge Graphene Centre, University of Cambridge, Cambridge CB3 0FA, UK
Dr. S. Afroj
Department of Engineering, Faculty of Environment, Science and Economy, University of Exeter, Exeter EX4 4QF, UK
Prof. N. Karim
Department of Fashion and Textiles, University of Southampton, Southampton SO23 8DL, UK
Nottingham School of Art and Design, Nottingham Trent University, Shakespeare Street, Nottingham NG1 4GG, UK
M. Dulal
Department of Textile Engineering Management, Bangladesh University of Textiles (BUTEX), Tejgaon Industrial Area, Dhaka-1208, Bangladesh
Dr. M. R. Islam
Department of Wet Process Engineering, Bangladesh University of Textiles (BUTEX), Tejgaon Industrial Area, Dhaka-1208, Bangladesh
The ORCID identification number(s) for the author(s) of this article can be found under https://doi.org/10.1002/eem2.12854.

DOI: 10.1002/eem2.12854

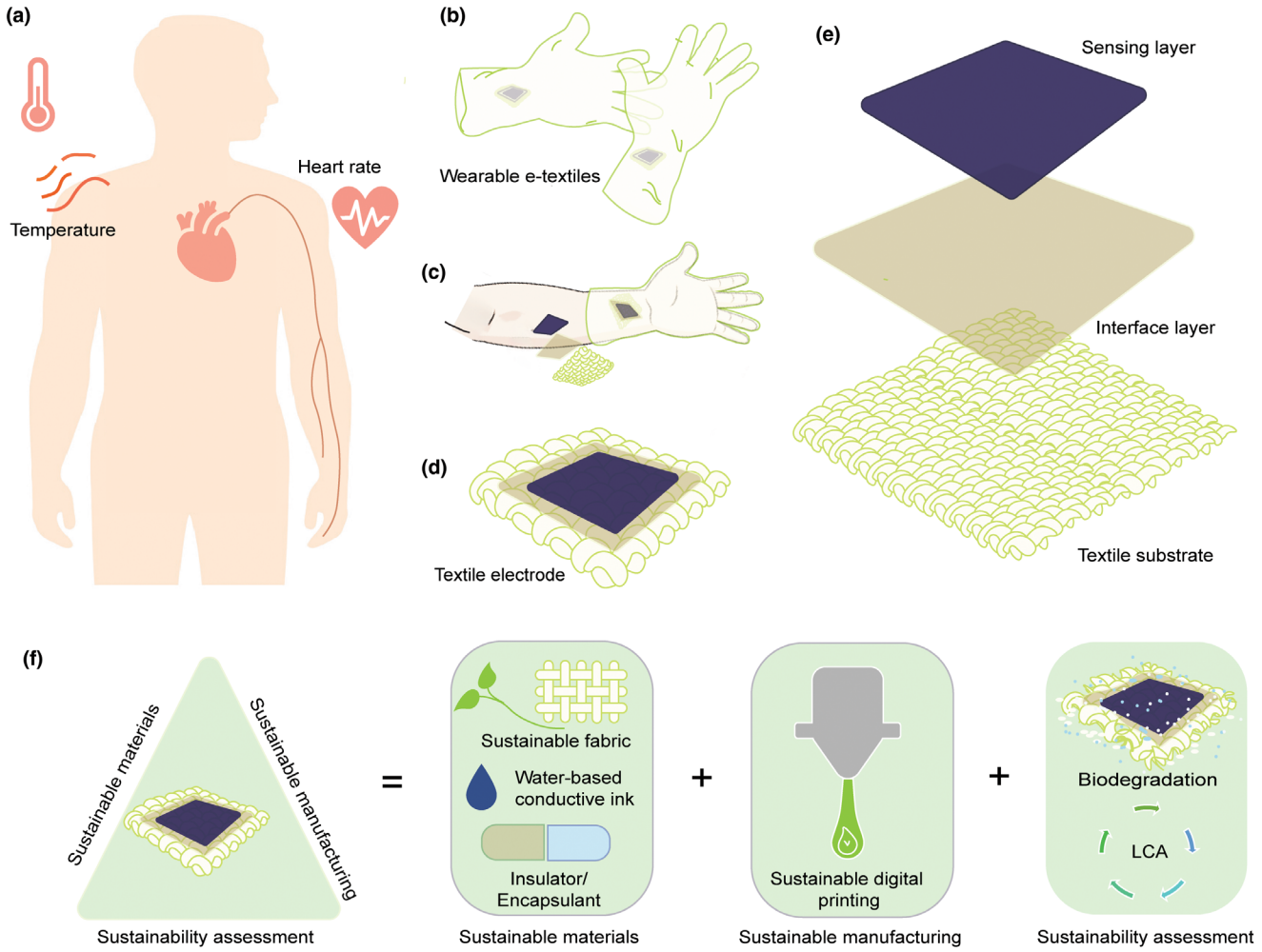

Figure 1. Toward sustainable wearable e-textiles for vital sign monitoring. a) Schematic of two important vital signs: skin surface temperature and heart rate of the human body. b) Schematic of wearable e-textiles as gloves. c) Schematic of the position of wearable textile electrode on human skin surface contact. d) Schematic of the textile electrode. e) Schematic of the textile electrodes' composition. f) Schematic of sustainable design approach for wearable e-textiles, including sustainable materials, sustainable manufacturing, and sustainability assessment.

growing demand for healthcare services, necessitates effective strategies for managing the health and well-being of older individuals. However, current clinics and hospitals rely on an array of sensors, wires, and cables connected to bedside monitors.[6] Fortunately, recent advances in e-textiles are leading to the development of a broad class of flexible, wearable, and skin-interfaced multifunctional sensors to address these limitations, with simple setup and use in the simultaneous acquisition of multiple signal classes.[7] However, the widespread adoption of e-textiles faces substantial challenges, including poor material performance and sustainability, intricate and time-intensive fabrication techniques, the generation of numerous toxic wastes during manufacturing, and limitations in end-of-life processing.[8,9]

Current e-waste comprises many materials like metals, glass, and plastics, each necessitating specific recycling methods due to their diverse physical and chemical properties.[10] This includes valuable components and hazardous materials such as heavy metals and halogenated organic compounds, posing risks to human health and the environment.[11] The difficulties in recycling e-textiles, or textiles coupled with electrical components, worsen this issue because valuable materials are typically dispersed in large amounts of heterogeneous textile waste. Typically, sorted materials are disposed of as solid waste. Technically, the existing waste electrical and electronic equipment (WEEE) take-back and recycling processes cannot handle this new kind of waste.[12] Therefore, there is an urgent, unmet need for a sustainable approach to integrated product design, the use of eco-friendly materials, sustainable manufacturing processes, and an effective end-of-life strategy to encourage the production of the next generation of smart and sustainable wearable e-textiles that can either be recycled to value-added products or decomposed in the landfill without any negative environmental impacts.

Here, we introduce the first sustainable approach of fabricating next-generation SWEET for continuous and concurrent monitoring of human vital signs including skin surface temperature and heart rate (**Figure 1**a). Our eco-friendly design approach for sustainable e-textiles includes: first, the use of sustainable textiles (Tencel)[13] due to their biodegradability, renewability, as well as softness and comfort along with eco-friendly electronic materials (graphene and PEDOT.PSS as active electronics and bioelectronic material,[14] respectively). Second, it

includes the use of high-precision and sustainable digital inkjet printing techniques for rapid, precise, and localized deposition of an exact amount of conductive electronic materials[15] on the textiles coupled with the benefits of direct (mask-free) patterning, comparatively higher resolution, minimal material waste, and exceptional compatibility with various active materials and substrates.[16] Finally, a holistic approach to sustainability analysis of e-textiles including biodegradability and LCA testing was undertaken because they provide a systematic and comprehensive way to understand, measure, and mitigate ecological and environmental impacts.[17] Our approach creates textile electrodes that can be sustainable by promoting microbial biodegradation and mitigating the environmental impact.

2. The SWEET Platform

The SWEET consists of a multi-layer sensing platform and attaches to textile gloves for monitoring human subjects' skin surface temperature and heart rate variability (Figure 1a,b). To develop sustainable wearable e-textiles, choosing the correct raw materials for the textile substrate is crucial, as fibrous materials are the fundamental building block in smart and wearable e-textiles.[18,19] Tencel™/Lyocell fabrics were used as the base substrate,[13] due to their environmentally friendly closed-loop production method with a higher resource efficiency (~99% recovery rate for water and solvent) and little negative environmental impact. However, all-inkjet-printed wearable e-textiles have been demonstrated mostly on cotton and polyester fabrics.[20] In the previous work, a CNT/PEDOT:PSS ink was deposited by inkjet printing onto adhesive polyamide-based taffeta fabric, creating a temperature sensor with a sensitivity of 0.31% $°C^{-1}$, effective from room temperature to 50 °C.[21] Additionally, ECG recordings from commercially available polyamide pantyhose with PEDOT:PSS-based dry textile electrodes showed indiscernible characteristic peaks,[22] indicating a need for more effective, environmentally friendly dry electrodes. To address this, we chose water-based PEDOT:PSS and formulated graphene inks, respectively, demonstrating their capabilities in vital sign sensing. Therefore, we optimized the electrical conductivity on the biodegradable Tencel fabric substrate for these two types of inkjet-printable conductive inks: PEDOT:PSS and graphene. This optimization aimed to develop a high-performance sensing layer that balances lower environmental impact and biodegradation behavior of e-textiles and toward a microbial community with multifunctional performance, advancing the state-of-the-art for ECG and temperature electrodes for vital sign monitoring upon skin contact. The composite inks containing PEDOT:PSS, seaweed cellulose, and glycerol were previously used as biodegradable conductive polymers, also this bioelectronic material-based augmentation can be considered a sustainable bridging technology, because it offers the possibility to decouple the service durations of disposable, and multi-use, quasi-permanent components,[14] where graphene is considered to be potentially more environmentally friendly than most commonly used non-biodegradable metals (e.g., Ag, Cu) for wearable e-textile application.[23] However, there remains a gap for a holistic approach to the sustainability assessment of fully-printed wearable e-textiles with PEDOT:PSS and graphene-based inkjet inks, which is addressed in this study.

Prior to the deposition of ink onto textiles *via* inkjet printing, the textile substrate underwent surface pre-treatment to ensure a continuous conductive track on a rough and porous textile surface, which is also essential to prevent delamination or detachment during use or washing. The drying time and temperature for water-based inkjet inks were optimized, which are biocompatible and use less energy for drying. Our fully inkjet-printed PEDOT:PSS- and graphene-based temperature and ECG sensors offer a sustainable solution to existing energy-intensive and time-consuming screen printing and coating processes with a huge waste of materials and water. Additionally, we tested the flexibility of textile-based inkjet-printed electrodes, which must keep their conductivity even after being flexed (Figure 1d,e).

We integrated these textile-based electrodes into a glove (Figure 1b, c) to demonstrate how the simultaneous use of wearable e-textiles on the human body can measure the skin surface temperature, ECG signal and heart rate. In addition, providing consistent and continuous vital sign monitoring with five participants. Alongside these electrode performance evaluations, our work showcases the sustainable design approach of wearable e-textiles through sustainability assessments aiming to advance the development of next-generation wearable e-textiles that are simpler, functional and less intrusive than current state-of-the-art materials/ electrodes, while also being environmentally responsible. To assess sustainability (Figure 1f), we performed a soil burial test of the inkjet-printed electrodes to determine the biodegradation behavior and the extent to which an electrode will degrade or disintegrate over time and to analyze the ecological impact *via* microbial enumeration of the soil around the buried samples to determine the effect of the textile on soil microbial communities and vice versa. Then LCA of inkjet-printed textile electrodes was tested to assess the environmental impact inside the system boundary.

3. Sustainable Inkjet-Printing of Wearable E-textile Sensors for Vital Sign Monitoring

Inkjet printing of electrically conductive pathways on textiles offers significant benefits,[24] including precise deposition of conductive materials, high-resolution printed electronics, and reduced material waste, **Figure 2**a. Despite these advantages, existing liquid phase exfoliation (LPE)-based graphene and other 2D material dispersions are less than ideal for wearable e-textile applications, due to the reliance on hazardous solvents, costly processing, and often higher drying temperature requirements. To address these challenges, biocompatible, water-based inkjet inks comprised of graphene were developed, avoiding severe conditions and chemical treatments. Additionally, Inkjet printing onto rough, porous textile surfaces poses challenges due to fiber orientation and morphology changes from water exchange.[24] To mitigate this, we pre-treated textile surfaces with a thin interface layer to reduce roughness, enabling the successful inkjet printing of continuous conductive tracks using PEDOT:PSS and graphene inks (Figure S4a, Supporting Information).

We optimized the electrical properties by varying the number of printed layers, observing an inverse relationship between the number of layers and resistance. Optimal resistances were achieved with 50 layers of PEDOT:PSS (~0.05 $k\Omega\,cm^{-1}$) and 120 layers of graphene (~2.9 $k\Omega\,cm^{-1}$), demonstrating stable electrical characteristics, Figure 2b. Curing time and temperature significantly impacted the resistance of the printed electrodes (Figure 2c,d), which were optimized and the optimal conductivity was achieved at 100 °C for 5 min. Higher temperatures and longer curing times increased resistance due to potential conductive ink and textile distortion from extreme heat. Additionally, flexibility tests (Figure 2f) revealed that our inkjet-printed

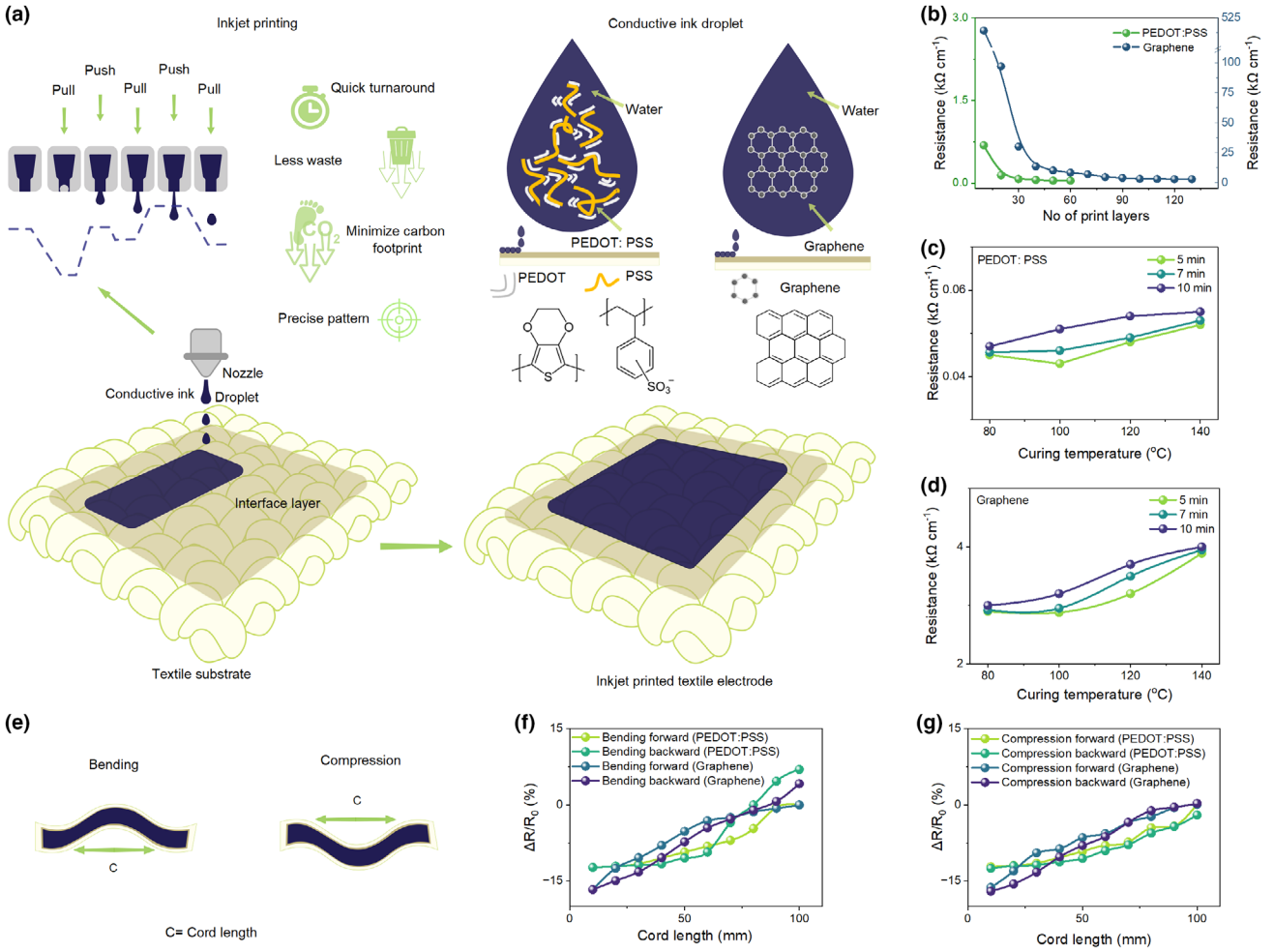

Figure 2. Inkjet-printed highly conductive wearable e-textiles. a) Schematic showing two water-based inkjet printable inks and drop-on-demand inkjet printing using a pull-and-push technique to showcase the advantages of inkjet printing and PEDOT:PSS and graphene's primary components, in droplets. b) The change in electrical resistance with the number of print layers via inkjet printing for PEDOT:PSS-and graphene- inkjet-printed conductive track. c) The change in electrical resistance of PEDOT:PSS- inkjet-printed conductive track with curing time and temperature. d) The change in electrical resistance of graphene- inkjet-printed with curing time and temperature. e) Schematic of flexible and wash stability of wearable e-textiles. f) $\Delta R/R_0$ change of the bending sensor in backward and forward direction for PEDOT:PSS and graphene- inkjet-printed wearable e-textiles (10 cycles). g) $\Delta R/R_0$ change of the compression sensor in backward and forward direction for PEDOT:PSS and graphene inkjet-printed wearable e-textiles (10 cycles).

textiles maintained consistent resistance changes ($\Delta R/R_0$) under mechanical stresses, such as bending and compression, indicating excellent flexibility for wearable applications, Figure 2e–g.

We first demonstrated the functionality of our inkjet-printed textile electrodes as ECG sensor to capture the electrical activity of the heart from several body sights to monitor heart function and detect pathology. These textile electrodes, when positioned on either arm (**Figure 3a**), measured the electrical activity produced by the heart's pumping action. Wearable devices are frequently worn on the wrist, where the radial artery is located close to the skin's surface.[25] In medical contexts, this artery is utilized to measure the pulse, and sensors can easily pick up the pulsations brought on by the heartbeat. The performance of the developed electrodes was compared with that of diagnostic tab electrodes as a reference in ECG recordings on human subjects. The amplitude and heart rate from the recorded signals, under a relaxed sitting position, were assessed. The morphology (appearance) of the waves and intervals, as shown in Figure 3b, illustrated a classic ECG curve required for ECG interpretation. Heartbeat is regulated (Figure 3c) by an electrical impulse that causes the characteristic reading of an ECG.[26] Figure 3d–f shows an ECG signal that was collected by reference electrodes and the electrode patches made of PEDOT:PSS and graphene, respectively, demonstrating their continued ability to detect cardiac impulses. Figure 3g demonstrates that the amplitude of the developed electrode patches matches that of the reference patch between 40 and 50 s, and more extended from 18 to 21 s in Figure 3h. Although the amplitude of the graphene inkjet-printed electrode for the same subject differs slightly from that of the reference and PEDOT:PSS inkjet-printed electrodes, the ECG pattern is made up of a recurring wave sequence of P, QRS, and T connected to each beat similar in appearance with an ideal ECG curve in Figure 3b. The intervals and amplitudes defined by these waves are necessary for some of the clinically useful information.[27] Figure 3i shows the heart rate in bpm

from the QRS complex of the ECG curve as the R wave, which stands for the depolarization of the heart's ventricles during contraction and has a noticeable peak in an ECG's QRS complex.

The average heart rate was determined to be 68 and 74 bpm from PEDOT: PSS and graphene inkjet-printed electrodes, respectively, whereas the reference electrode gave a heart rate of 70 bpm. Reference and PEDOT:PSS electrodes have better conductivity and low skin contact impedance compared to graphene-inkjet-printed electrodes. ECG electrodes can produce more precise, consistent, and dependable readings by ensuring low skin contact impedance, which is essential for efficient cardiovascular monitoring and diagnostics.[28] For instance, graphene-inkjet-printed textile electrodes showed an impedance range from 1374 kΩ (at 10 Hz) to 34.6 kΩ (at 1 kHz) upon skin contact, whereas PEDOT:PSS and reference electrodes exhibited an impedance range from 291.4 and 24.1 kΩ (at 10 Hz) to 17.4 and 3.1 kΩ (at 1 kHz). Higher impedance in electrodes could lead to a higher amplitude of the recorded signal due to increased resistance. Additionally, dry textile electrode compatibility on the skin affects signal quality, potentially increasing noise and altering the amplitude and R-R interval measurements.[29] The ECG waveform's overall appearance may therefore change because of these variations in R wave spacing. Other factors, such as the subject's physiological state and electrode positioning, and uniformity of contact pressure may cause variations or discrepancies in the ECG curve from the same participant due to time differences in wearing. Despite the higher impedance of our inkjet-printed dry electrodes compared to reference gel types, they remain within the acceptable impedance spectrum for dry electrodes as large as several hundred kilo-ohms to mega-ohms,[30] validating their accuracy and dependability and viability for ECG monitoring with enhanced user comfort demonstrating the potential of our textile electrode *via* skin-electrode interface as a step toward personalized healthcare applications by meeting up requirements[30,31] of wearer convenient flexible, effective ionic current flow and signal acquisition. The obtained results are encouraging, providing a pathway for the development of wearable e-textiles for covert ECG monitoring and for the expansion of their use to capture additional bio-potentials.

We then used inkjet printing to fabricate our developed PEDOT:PSS and graphene inkjet-printed temperature sensing layer on textiles and the sensitivity from the prepared electrodes was determined by TCR value. Figure 3j illustrates the sensitivity measurement connection setup on a hotplate where the temperature was set to rise to ∼40 °C. To determine whether the developed electrode sense skin surface temperature close to human body temperature. It was evident that both temperature sensors PEDOT:PSS and graphene showed negative relative resistance changes with increasing temperature (Figure 3n), indicating a decrease in electrical resistance when heated and vice versa when cooled. The graphene inkjet-printed temperature sensor demonstrated a rapid resistance change, whereas the PEDOT:PSS-based sensor showed a steeper increase in resistance. The response time required to reach from room temperature to ∼40 °C for PEDOT:PSS was 102 s and for graphene 88 s (Figure 3o). Figure 3p shows the repeatability test of temperature between ∼25 and ∼40 °C by heating and cooling each electrode over the hot plate. The minimal response fluctuations in relative resistance change across various cycles near 40 °C from room temperature indicated consistent sensor performance throughout multiple cyclic tests within the same temperature range. Also, the sensors exhibited good sensing performance with only a very slight variation when brought from a temperature of ∼40 °C to room temperature, with a relative resistance change of between ∼2.6% and ∼1.2%. A textile-based sensor patch attached to the glass jar could give clear monitoring of resistance change when adding hot water (Figure 3k) to demonstrate the temperature sensing capability at different stimuli. It was observed from Figure 3q that on adding hot water to the jar there was a rapid change of relative resistance in the PEDOT:PSS and graphene temperature sensors, requiring almost 30 s to reach a plateau value.

The temperature sensors were examined in the user interface software, with the findings being assessed using the MAX 30205 EVE kit as a reference (Figure 3l). Within 100 s, textile-based PEDOT and graphene inkjet-printed sensors (Figure 3r) stabilized at 27–29 °C and 30–31 °C, respectively, which is comparable to the reference's 28 °C. As seen in the schematic in Figure 3m responding to human skin surface temperature, the sensors showed a negative temperature coefficient of resistance (NTC) with values of −4.8 and −5.0% $°C^{-1}$ for PEDOT and graphene, respectively (Figure 3s) as electrical resistance decreases with rising temperature upon skin contact (from ∼0.043 to ∼0.02 kΩ cm^{-1} for PEDOT and from ∼2.88 to ∼1.28 kΩ cm^{-1} for graphene). This occurrence may happen from improved charge carrier transit and production under thermal stimuli in PEDOT:PSS-inkjet-printed sensors,[32] attributed to their core-shell grain structure, while graphene's exceptional properties, including high thermal conductivity[33] and temperature-responsive behavior,[34] make it an excellent candidate for temperature sensing applications with negative TCR.

4. Concurrent Monitoring of Vital Signs Via the SWEET Platform

The conductive components on textile platforms were incorporated to develop diverse applications.[9] This has led to the perception of these wearable e-textiles as prospective substitutes for expensive analytical tools used in sports, medicine, or the biomedical industries for the monitoring of physiological profiles. In the previous section, we demonstrated the inkjet-printed PEDOT:PSS and graphene electrodes separately for ECG signal capturing and temperature sensing capabilities. To show that these electrodes can function effectively when integrated into a textile product, we tested their ability by integrating them into textile gloves (**Figure 4**a) to monitor vital signs (temperature and heart rate), illustrated in Figure 4b, upon contact with the human skin surface, confirming the concurrent monitoring capability of the developed electrodes from a single product which facilitates convenient data collection and enhances subject comfort.

The findings showcased in this study center on the adaptation and optimization of this technology specifically for monitoring ECG and their synchronization concerning different phases, such as relaxed sitting and jogging. Notably, during jogging, higher amplitude intensities were observed compared to when in a relaxed sitting position, both using the same gloves with electrodes near the wrist. This study examined the R-R intervals, and heart rates recorded from the textile-electrode wrist device, showcasing ∼0.94 s and 64 bpm from PEDOT:PSS inkjet-printed and ∼0.82 s and 74 bpm from graphene inkjet-printed, respectively. Moreover, a comparison with a commercial tab, as depicted in Figure 3g,h, showed an error of ∼0.10 s and ∼4 bpm from both kinds. These results highlight the effectiveness and reliability of these electrodes' sensing capabilities. The ECG signal was detected simultaneously, depicted in Figure 4d, where the amplitude of the ECG curve closely aligns with the patch's amplitude, as previously discussed (Figure 3g,h). An expanded view in Figure 4e highlights three prominent R waves between 27 and 30 s, maintaining an effective heart rate detection using wearable e-textiles based on PEDOT:PSS and graphene

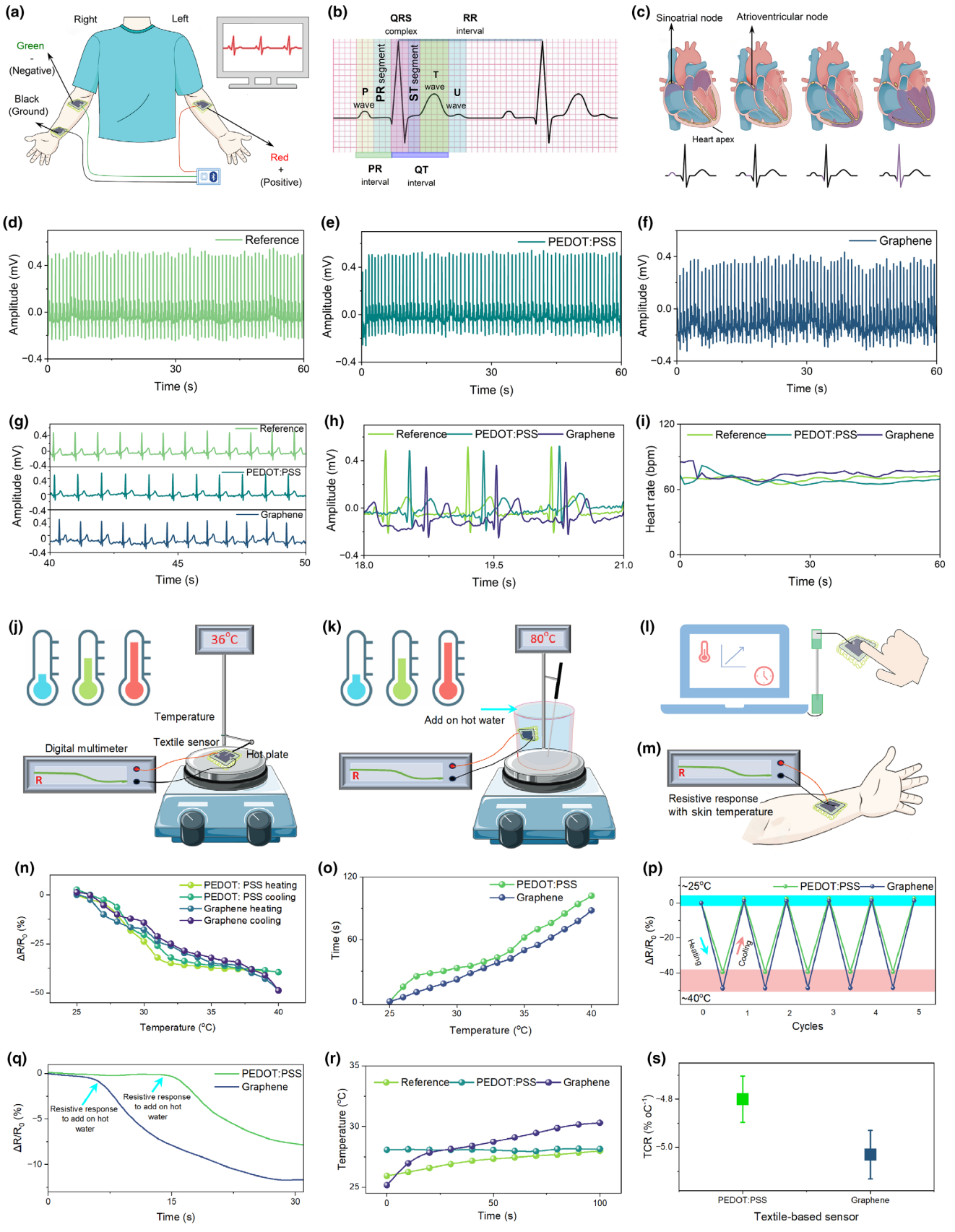

Figure 3. Inkjet-printed wearable e-textiles for vital sign monitoring. a) Schematic of textile electrodes patches positioning on subject's right and left hands and connecting with reference device for ECG signals. b) Schematic of a normal ECG curve with P wave, QRS complex, T wave, U wave, PR segment, ST segment, PR interval, QT interval and RR interval. c) Schematic of one heartbeat cycle. d–f) ECG signal captured for 60 s of subject (sitting) from reference, PEDOT:PSS and graphene inkjet-printed electrodes, respectively. g) Expanded version of d–f) from 40 to 50 s. h) Expanded version of d–f) from 18 to 21 s. i) Heart rate measured in bpm for 60 s of subject (sitting) from the QRS complex reading of d–f) from reference, PEDOT:PSS and graphene inkjet-printed electrodes, respectively. j) Schematic of hot-plate and digital multi-meter set-up connection with inkjet-printed textile electrode for characterizing the effect of resistance change due to heating and cooling. k) Schematic diagram of sensing platform on a glass jar for real-time object temperature monitoring. l) Schematic of MAX30205 human body temperature sensor evaluation kit connection with inkjet-printed textile electrode to show the change of body temperature with time. m) Schematic of resistive response of inkjet-printed textile electrode with skin surface temperature. n) $\Delta R/R_0$ change of PEDOT:PSS and graphene inkjet-printed textile electrode with heating and cooling. o) Response time to reach the set temperature on hot plate for PEDOT:PSS and graphene inkjet-printed textile electrodes. p) $\Delta R/R_0$ change of PEDOT:PSS and graphene inkjet-printed textile electrodes for 5 cycles from low to high temperature via heating and from high to low temperature via cooling. q) The effect of $\Delta R/R_0$ with time at adding hot water onto glass jar. r) Temperature reading of skin surface within 100 s of reference MAX30205 evaluation kit, PEDOT:PSS and graphene inkjet-printed textile electrodes. s) TCR value of PEDOT:PSS and graphene inkjet-printed textile sensor.

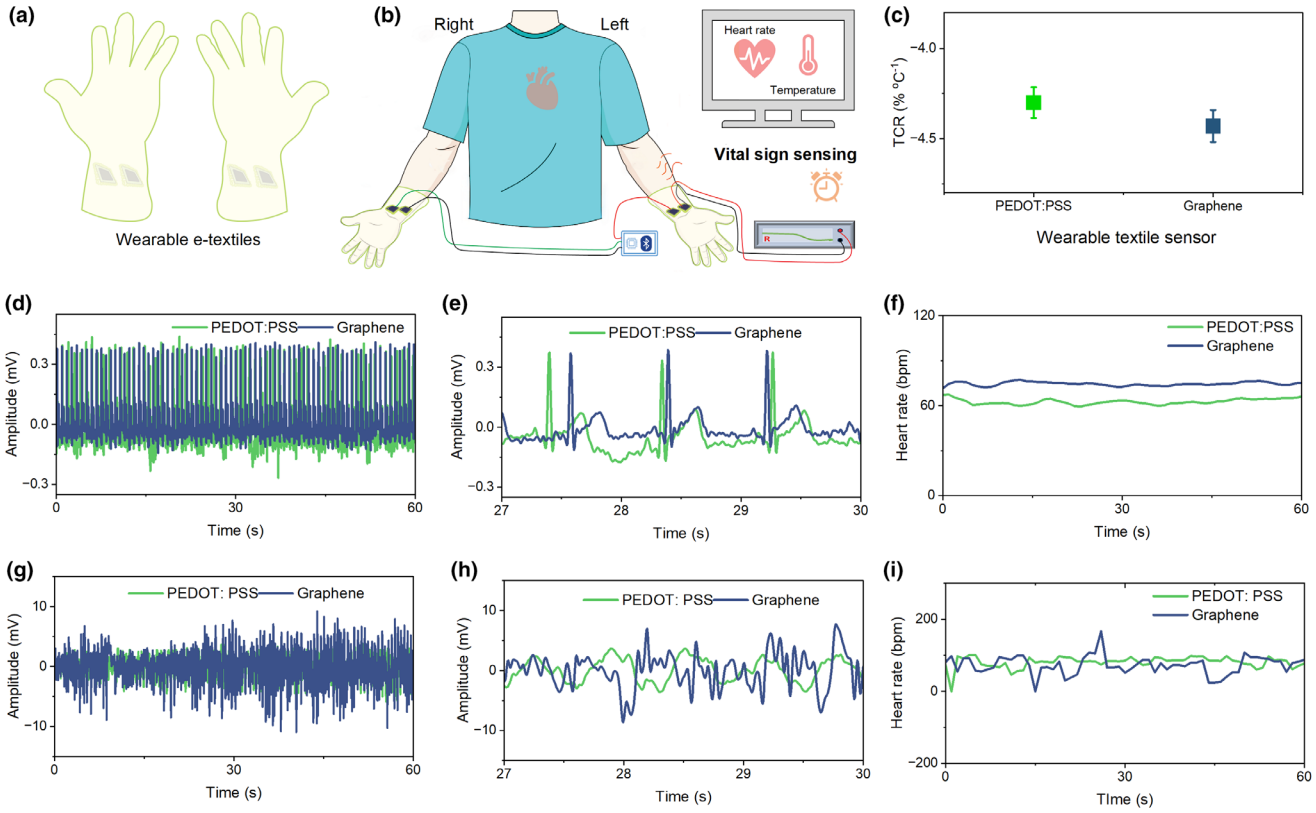

Figure 4. Concurrent monitoring of vital signs *via* SWEET platform. a) Wearable e-textiles where textile electrodes are attached to textile gloves. b) Schematic of concurrent performance measuring set up with wearable e-textiles worn by subject. c) TCR value of wearable textile sensor composed of PEDOT:PSS and graphene inkjet-printed respectively. d) ECG signal captured for 60 s of subject (sitting) from PEDOT:PSS and graphene inkjet-printed wearable e-textiles respectively. e) Expanded version of d) from 27 to 30 s. f) Heart rate measured in bpm for 60 s of subject (sitting) from the QRS complex reading of d) from PEDOT:PSS and graphene inkjet-printed wearable e-textiles respectively. g) ECG signal captured for 60 s of subject (jogging) from PEDOT:PSS and graphene inkjet-printed wearable e-textiles respectively. h) Expanded version of g) from 27 to 30 s. i) Heart rate measured in bpm for 60 s of subject (jogging) from the QRS complex reading of g) from PEDOT:PSS and graphene inkjet-printed wearable e-textiles respectively.

inkjet printing. Additionally, Figure 4g,h illustrates the shift in the ECG curve, whereas Figure 4i displays the corresponding change in heart rate as the subject transitions from a relaxed sitting posture to jogging for a minute.

Moreover, the TCR in PEDOT:PSS and graphene inkjet-printed textile electrodes changes from enhanced charge carrier mobility as temperatures increase, resulting in diminished electrical resistance within their structures. This phenomenon allows these materials to exhibit decreased resistance as temperatures increase, contributing to their negative TCR properties. Figure 4c demonstrates the closely aligned TCR values for wearable e-textiles produced using inkjet-printing methods with PEDOT:PSS and graphene. These values, averaging ∼−4.3 and −4.43, respectively, were observed while the subject was in a relaxed seated position, wearing gloves with integrated electrodes which is

comparable to a commercially available epoxy-coated NTC Thermistor Cable as a reference temperature sensor. Upon the subject wearing these gloves, electrode resistance decreased due to the transition from room temperature to the subject's temperature upon skin contact. Hence, our fabricated e-textiles offer a sustainable alternative for continuous physiological monitoring, reducing the need for intrusive sensors and enhancing user comfort. The integration of our developed textile electrodes into clothing enables vital sign detection, supporting continuous monitoring from lab to life and promoting the advancement of smart clothing technologies with sustainable materials. This

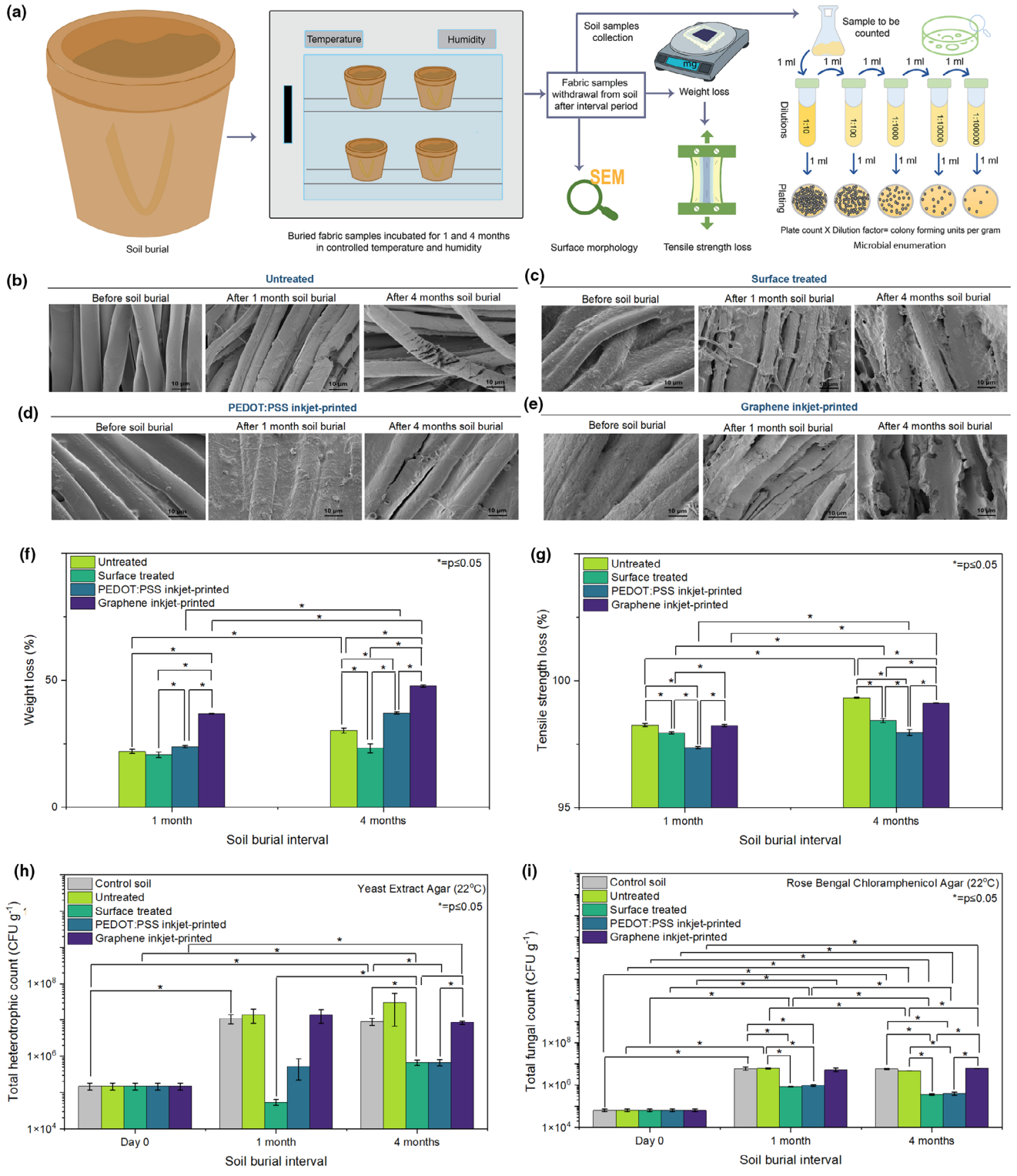

Figure 5. Biodegradation behavior analysis of wearable e-textiles and its impact on soil microbial population. a) Schematic of unglazed pottery with buried sample under controlled temperature and humidity in incubator, showing subsequent surface morphology test, weight loss, tensile strength loss measurement and serial dilution to determine viable micro-organisms in soil. Scanning electron microscope (SEM) images (×2500) of before and after 1 and 4 months soil burial of respectively: b) Untreated fabric, c) Surface treated fabric, d) PEDOT:PSS inkjet-printed conductive track over surface treated fabric, e) Graphene inkjet-printed conductive track over surface treated fabric. 1 and 4 months soil burial effect of untreated fabric, surface treated fabric, PEDOT:PSS inkjet-printed conductive track over surface treated fabric, Graphene inkjet-printed conductive track over surface treated fabric, respectively: f) Weight loss (%), g) Tensile strength loss (%). Microbial viable count from soil samples: control soil and the soil of 1 and 4 months soil burial of untreated fabric, surface treated fabric, PEDOT:PSS inkjet-printed conductive track over surface treated fabric, Graphene inkjet-printed conductive track over surface treated fabric: h) Total heterotrophic plate count (bacteria and fungi; mean ± SD), i) Total fungal count (mean ± SD). *Significant differences observed between samples ($p \leq 0.05$).

approach aligns with the growing demand for simplified, miniaturized technology and paves the way for future endeavors that use clothing as a medium in confined signal transmission through wearable electronics.[35–40]

5. Biodegradation Behavior of Wearable E-textiles and its Impact on Microbial Enumeration

Amid rising pollution from landfills and the atmosphere, our study addresses the lack of research on both the biodegradation of wearable e-textiles and their environmental impact on soil microflora, focusing on integrating sustainable fibers and conductive ink in the e-textile design. The biodegradation behavior of a sustainable textile-based inkjet-printed electrode made of PEDOT:PSS and graphene ink, respectively, and its impact on microbial communities in soil are reported at two different time intervals (**Figure 5**a). After 1 and 4 months of soil burial, the test fabrics were visually examined, and weight and tensile strength losses were established. Scanning electron microscopy (SEM) was used to assess the textile electrodes' propensity for biodegradation (Figure 5b–e) and compared against standard control fabrics.

Biodegradation assessments of materials like fibers and textiles involve initial visual inspection, as shown in Figure S6d–g, Supporting Information, which compares fabric conditions before and after soil burial. The 4-month burial image of the untreated fabric shows deeper holes along with yellowing, fraying, and tearing, whereas the 1-month burial image shows tiny holes. On the other hand, because the PEDOT:PSS and graphene inkjet-printed track pigments disintegrated, the 4-month burial image of the PEDOT:PSS and graphene inkjet-printed conductive track pigments had more flecks and color fading than the 1-month burial image. The color of the surface-treated fabric turns yellowish in comparison to before burial between 1 and 4 months after burial, however there is little change in color between the intervals.

However, fabrics with graphene inkjet-printed tracks underwent visible degradation, reflecting the associated weight loss (∼36.89% and ∼47.73% after 1 and 4 months of soil burial, respectively) observed in Figure 5f. When compared to the fabric before soil burial, the surface morphology of the fabric samples after soil burial showed obvious deterioration and changes after 1 and 4 months, as illustrated by untreated, surface treated, PEDOT:PSS inkjet-printed and graphene inkjet-printed materials, respectively (Figure 5b–e). The surface solvent-interface layer on the treated fabric served as a protective barrier, limiting degradation even after 4 months of soil burial, as evidenced by its minimal weight loss compared to untreated and inkjet-printed fabrics. The analysis of Figure 5f showed that after 1 month, weight loss in surface-treated fabric, with or without PEDOT:PSS ink, was not significantly different from untreated fabric. However, the graphene inkjet-printed fabric displayed notable weight loss, suggesting material-specific interactions with the treatment layer. This difference may arise from the unique properties and environmental responses of PEDOT:PSS and graphene materials, affecting their compatibility and adhesion to the treated fabric. Graphene inkjet-printed fabric showed increased weight loss during soil burial compared to untreated fabric, likely due to graphene's larger surface area and higher susceptibility to soil degradation processes.[41] The behavior of graphene ink, explored by expanding the printing process to 120 layers, revealed that graphene's absorption into fibers and subsequent adsorption onto surfaces initially reduces resistance and forms a conductive layer. However, the unadsorbed graphene may break down in the soil, contributing to weight loss, while the absorbed graphene maintains structural integrity, initially preserving tensile strength. Over time, extended exposure leads to tensile strength loss significantly (∼98% and above) across all fabric types, as evidenced in Figure 5g and in the load–displacement curve of Figure S7, Supporting Information.

Prior to the widespread adoption of wearable e-textiles with materials like PEDOT:PSS, graphene; exposure of these materials to the environment is a critical consideration. The soil environment, being a prominent part of the natural ecosystem, is particularly susceptible to pollutant exposure.[42] Therefore, it is imperative to understand the environmental transformation behavior of graphene and PEDOT:PSS. To assess the impact of these materials on microbial communities, the soil around where fabric samples were buried was examined to determine the total heterotrophic viable count (the combined bacterial and fungal population of the soil; Figure 5h and Figure S8a, Supporting Information), total viable fungal count (Figure 5i and Figure S8b, Supporting Information), and the total viable bacterial count recovered under low nutrient conditions (Figure S8c,d, Supporting Information). This investigation is essential to ensure the compatibility and sustainability of wearable e-textiles in diverse environmental conditions. These findings provide new insights into environmental behaviors of nanomaterials and bioelectronics. The results as depicted in Figure 5h,i and Figure S8a–d, Supporting Information, which indicate that microbial levels increase over time in the soil after 1 month, and then subsequently decrease or remain constant after 4 months. Interestingly, after 1 month burial only the surface treated fabric (Interface Layered Fabric) resulted in a reduced total heterotrophic plate count. Therefore, indicating that the presence of the solvent-based interface layer as surface treatment has a detrimental effect on the bacterial population within the soil ecosystem. This could imply that the surface treatment may have bacteriostatic properties and/or provide lower readily available sources of nutrients (e.g. carbon) for microbial growth.

Nonetheless, the fungal levels in the soil with the solvent materials are relatively higher compared to the total heterotrophic plate counts, indicating that fungi are better adapted to surviving in the presence of solvent materials. Given the nature of the fabric, the variations in the microbial levels indicate that the composition of the fabric likely affects the total available carbon to the micro-organisms and either increases

or decreases their subsequent proliferation. This is consistent with other studies which attribute the structure of the textile to be linked to nutritional availability which in turn affects microbial growth.[43] The finding indicates that natural compounds, i.e. fabric and graphene, promote the bacterial and fungal composition of soil, while the solvent-based compounds, i.e. interface layer for surface treatment and PEDOT:PSS, promote only the fungal composition of soil (albeit to a lesser degree). The study results indicate that for solvent-based compounds, it is likely that as the synthetic components are degraded, the bacterial communities now have access to the more natural fibers thus allowing their growth from 1 to 4 months. During this same period, the fungal population remains relatively constant, which could be attributed to increased competition from bacteria once the more natural fibers are exposed. For natural materials, the initial available carbon is sufficient to cause an accelerated growth of the bacterial population causing a higher initial number, followed by a decline as the soil nutrients are depleted. This can be further mapped to the weight loss observed in this study (Figure 5f). The statistically significant differences observed between individual samples within this study demonstrates the variable effects textiles and e-textiles have on the environment, and this area of research necessitates further study to determine their impact on soil eco-systems (Figure 5h,i and Figure S8, Supporting Information). Furthermore, the effect soil micro-organisms have on the e-textile and its subsequent degradation can be a potential avenue to explore for accelerated biodegradation and even as potential power sources (bio-batteries/microbial fuel cells).[44]

6. Life Cycle Assessment (LCA) of Wearable E-textiles

LCA has been widely used to provide a systematic and reliable scientific foundation for assessing the environmental performance of production techniques from a systemic perspective,[45] and it has been positioned as a vital tool for environmental assessment. According to ISO 14040 and 14044 standards and frameworks,[46,47] the LCA methodology as a prospective approach was used in this case for the PEDOT:PSS and graphene inkjet-printed textile electrode of a rectangle conductive track of 10 cm × 1 cm area. In this study, laboratory-scale LCA of the selected and formulated materials for fabricating textile electrodes (System boundary, **Figure 6a**) was conducted to evaluate their environmental performance to that of a reference metal/solvent-based printed textile electrode. This particular focus makes it possible to analyze the inventory in the fabrication process in more depth and under control. Conducting a life-cycle inventory (LCI) involves collecting extensive input–output data about the activities within the defined system boundary, including textile substrate, interface layer, conductive ink (see Table S2, Supporting Information). This LCA modeling process requires a meticulous selection of pertinent information on these inventories from Ecoinvent 3.6. The inventory, which is not included in the database, is the general synthesis route considering the proper raw materials used in LCA. And the impact assessment of these inventories by SimaPro software using ReCiPe2016 method shows that the polymer PEDOT:PSS and graphene inkjet-printed textile electrodes have a lower normalized value of total impact when compared to the reference metal/solvent-based textile electrode, as illustrated in Figure 6b. Out of all the indicators, it was found (Figure S9, Supporting Information) that marine ecotoxicity had the greatest impact (~65%) on the reference textile electrode due to a hazard-weighted rise in marine water. In particular, the PEDOT:PSS inkjet-printed textile electrode had a ~28% negative impact on freshwater eutrophication. According to study,[48] this factor described the lack of species as a result of phosphorus concentrations in freshwater, but it does depend on the type of freshwater (lakes or rivers), the group of species (heterotrophs and autotrophs), and the environment (warm, temperate, xeric, or cold). It shows the change in the potentially extinct proportion of species due to a change in total P concentration. Apart from this, water usage was significant compared to other indications for graphene inkjet-printed electrode, despite the fact that the water consumption was twice as low as that of the market available reference metal/solvent-based ink-printed textile electrode (Figure 6h). For a wider comparison, we have also shown the impacts among the electrodes (Reference, PEDOT:PSS, Graphene inkjet-printed) for the significant indicators in Figure 6c–h.

Within our lab scale system boundary of LCA from cradle to grave (Figure 6a), we identified a fully printed textile electrode with a defined pattern and area of optimized resistance which requires components including a textile substrate, an interface layer, and inkjet printable ink. It is evident the graphene and PEDOT:PSS inkjet-printed textile electrodes have the least impact overall, according to the impact assessment of textile electrodes based on this amount of material used in the fabrication process. In Figure 6g, it is evident the graphene inkjet-printed textile electrode had the lowest overall climate change impact of 0.037 kg CO_2 eq, which is ~40 times (97.5%) and 3 times (70.8%) lower than the reference and PEDOT:PSS inkjet-printed textile electrodes, respectively. Also, it has (1.53×10^{-4} kg SO_2 eq) the lowest impact on terrestrial acidification, compared to the reference (0.01 kg SO_2 eq) and the PEDOT:PSS (5.37×10^{-4} kg SO_2 eq) inkjet-printed textile electrodes. Figure 6f shows that reference-textile electrode (0.062 kg 1,4-DB eq) generates significantly greater outputs than the PEDOT:PSS inkjet-printed (6.73×10^{-4} kg 1,4-DB eq) and graphene inkjet-printed (2.74×10^{-4} kg 1,4-DB eq) electrodes, with its greater production of carcinogenic toxins. The latter electrodes may involve less harmful chemical syntheses with the associated emission of solvent, metal and organic catalyst. From the results, it is apparent that compared to solvent-based inks, which may contain hazardous chemicals, water-based inks are typically non-toxic and less detrimental to human health.[49] This is an important factor for workers in these manufacturing and printing sectors who are potentially exposed to these inks. Additionally, water-based inks have less of an adverse effect on the environment since they typically discharge less harmful chemicals into ecosystems and waterways. Solvent-based inks have a greater potential to pollute water and destroy marine life.

7. Conclusions

Electronics and sensor advancements of today need to concentrate on lowering environmental effects during a device's whole life cycle in addition to improving device performance. Currently, in this study we demonstrate PEDOT:PSS and graphene inkjet-printed wearable e-textiles, respectively capable of simultaneous ECG signal and skin surface temperature sensing with a measurement accuracy comparable to the state-of-the-art materials. Our findings show that the graphene inkjet-printed textile electrode biodegrades to ~98% decrease in tensile strength and ~48% reduction over 4 months. Also, naturally occurring substances such as Tencel fabric and graphene promote the presence of both bacteria and fungi in soil. Our design shows that graphene has ~70.8% lower global warming potential than PEDOT:PSS and ~97.5%

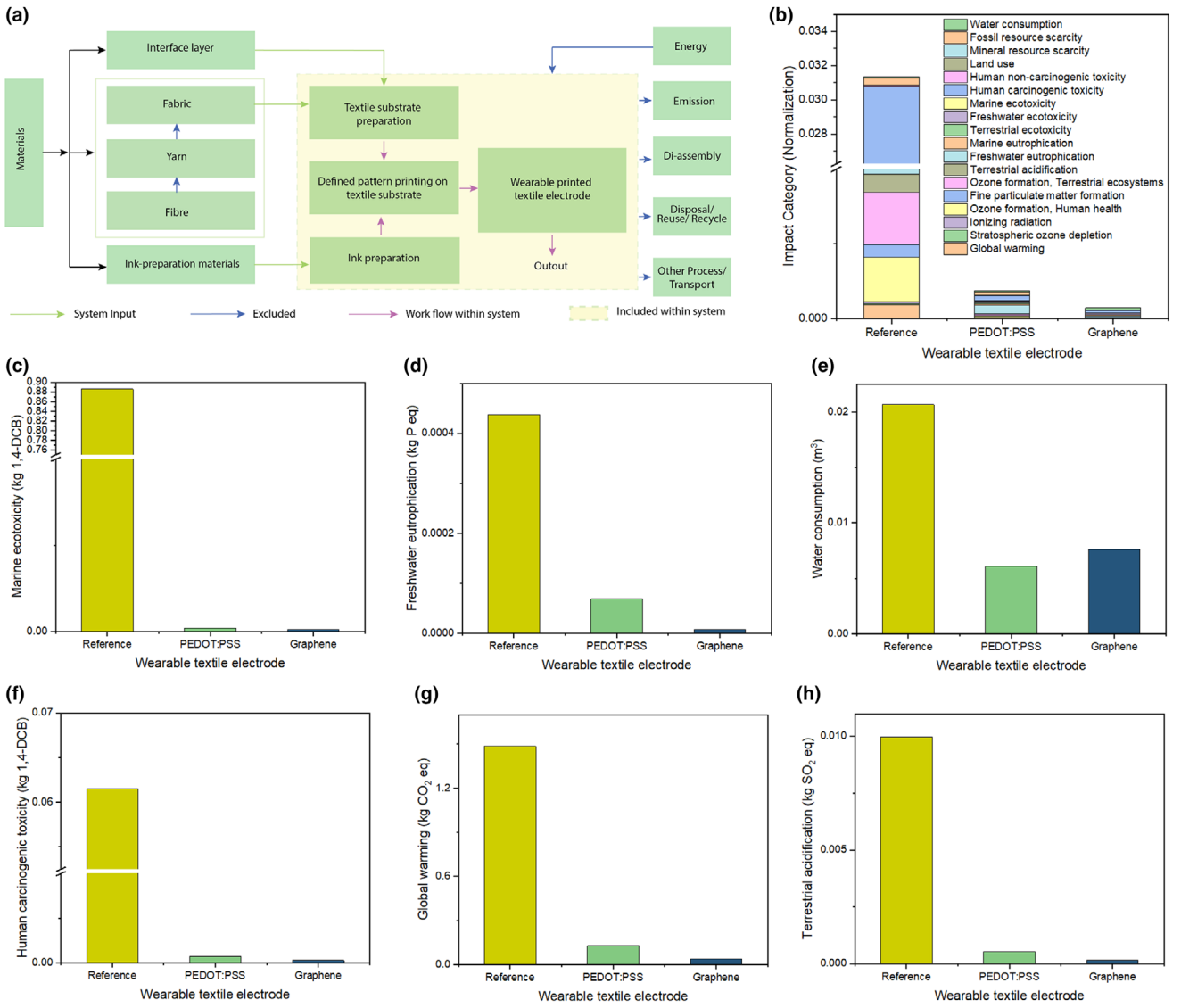

Figure 6. Life cycle assessment (LCA) of wearable e-textiles. a) System boundary of operational activities in laboratory scale. b) Impact category with normalized value for reference, PEDOT:PSS and graphene inkjet-printed textile electrodes. Comparison of marine ecotoxicity, freshwater eutrophication, water consumption, human carcinogenic toxicity, global warming and terrestrial acidification c–h) respectively for wearable textile electrode: reference, PEDOT:PSS- and graphene inkjet-printed.

lower than the reference material per textile electrode, highlighting its promise for the generation of sustainable platforms for real-time health monitoring. Our research contributes to the advancement of sustainability assessments for materials and manufacturing processes, nevertheless, by tailoring materials, design patterns, and directions to specific application requirements, it is still viable to develop an integrated product design that is completely biodegradable or recyclable and environmentally sustainable.

8. Experimental Section

Materials: The Tencel fabric was supplied from Nice Denim Ltd., Bangladesh. Dycotec Materials (DM-INS-2510) supplied the insulator paste, used as an interface layer for surface pre-treatment, which is applicable as a screen printable coating that is used in stretchable applications such as wearable devices, sensors, and medical devices. Graphite flakes, grade 3160, were purchased from Sigma Aldrich, UK. The following materials for graphene ink formulation were purchased from Sigma Aldrich (UK): 1-pyrenesulfonic acid sodium salt (PS1), suitable for fluorescence, ≥97.0% (HPLC); propylene glycol (P4347); Triton™ X-100 (laboratory grade), Xanthan gum and poly (3,4-ethylenedioxythiophene):poly (styrene sulfonate) 0.8% in H_2O conductive inkjet ink (739316). At 22 °C, the viscosity, surface tension and density of PEDOT:PSS in 0.8% H_2O was found to be $\eta_p \sim 9$ mPa s, $\gamma_p \sim 32.54$ mN m^{-1}, $\rho_p \sim 0.985$ g cm^{-3}, respectively. PEDOT:PSS inkjet printable ink was printed without any modification for drop ejection. Cardinal Health™ Kendall™ 5400 Diagnostic Tab Electrodes [Silver/Silver Chloride (Ag/AgCl)] were used as reference electrodes and purchased from Vernier, UK. Epoxy Coated NTC Thermistor Cable (TCR −4.4% $°C^{-1}$, given in the datasheet) was supplied by Molex (India). Yougarden Professional Grade Compost, purchased from Wilko, UK, was used for soil burial tests (with 50% composted wood fiber and a blend of white and green peats). Ethanol klercide™ (70/30 denatured ethanol) was purchased from Ecolab (UK) and was used to clean the fabric

samples. Ringer's solution, Yeast Extract Agar (CM0019B) and R2A agar (CM0906B) and Rose Bengal Chloramphenicol Agar (CM1148B and SR0078E) were supplied from ThermoFisher Scientific™ (UK).

Surface pretreatment of textiles: Printing low-viscosity inkjet inks onto a permeable textile surface using inkjet technology presents a significant difficulty, mainly because of the ever-shifting arrangement of fibers or yarns and the continuous alteration of fiber structure caused by the interaction of water molecules with the environment.[50] To address these challenges, an interface layer was applied for surface pre-treatment on the rough and porous textile substrate before inkjet printing of graphene and PEDOT:PSS inks, respectively, enabling the successful inkjet printing of continuous conductive tracks (Supporting Information). For one screen-printing pass (thread count 62T) of the interface layer onto the textile with the screen-printable insulator paste[51] yielding a rough thickness of 0.292 mm of fabric. The substrate was then dried at 100 °C for 10 min.

Graphene inkjet-printable ink preparation: A previously reported[52,53] liquid phase exfoliations (LPE) developed was used in this study as follows: a vial containing graphite powder (3 mg mL^{-1}), PS1 (1 mg mL^{-1}) and deionized water was sonicated at 600 W using a Hilsonic bath sonicator (UK) for 120 h at 15 °C. The liquid obtained was centrifuged using a ThermoFisher Scientific centrifuge to separate out and discard the residual non-exfoliated bulk flakes at 685 *g* and 3500 rpm speed for 30 min before collecting the upper 2/3 of volume to ensure only flakes of the correct lateral size (<580 nm, Figure S1, Supporting Information) were collected. The lower 1/3 fraction was collected to be used for the preparation of other batches of ink. To lower the risk of nozzle clogs, flakes with the proper lateral size were recovered by differential centrifugation. The collected supernatant was then centrifuged twice at 10 956 *g* and 14 000 rpm speed for 2 h to remove excess PS1 from the dispersion and the precipitate was then washed twice and re-dispersed in the printing solvent. The solvent was prepared as follows: 10 mL of Propylene Glycol, 10 mL of Xanthan gum and 6 mg of Triton™ X-100 was added to 100 mL of water and stirred to obtain a uniform printing solvent. The ink concentration was adjusted to 1 mg mL^{-1}. The graphene ink viscosity and surface tension were measured using a HAAKE Viscotester iQ Rheometer (ThermoFisher Scientific, UK) and a tensiometer (Theta Lite, Biolin Scientific, Sweden). The rheological parameters of graphene dispersions were modified using a non-ionic surfactant (Triton™ X-100), a viscosity modifier (Propylene Glycol), and thickening agent (Xanthan gum) to obtain $\eta_G \sim 4.2$ mPa s (Figure S2, Supporting Information), $\gamma_G \sim 33.98$ mN m^{-1} (Figure S3, Supporting Information), and $\rho_G \sim 1$ g cm^{-3}, providing a Z value ~6.43 (where $\alpha = \sim 21.5$ µm) for the formulated graphene inks.

Inkjet printing: A Dimatix DMP-2800 inkjet printer from Fujifilm Dimatix Inc. (Santa Clara, USA) was used to print PEDOT:PSS and graphene on a pretreated textile fabric, respectively. This printer can create and define patterns over an area of 200 mm × 300 mm and handle substrates up to 25 mm thick, being adjustable in the Z direction. The printer was equipped with a disposable piezo inkjet cartridge and the nozzle plate consists of a single row of 16 nozzles of ~21.5 µm diameter spaced 254 µm with a typical drop diameter ~27 µm and 10 pL drop size. Print head height was adjusted to 1.5 mm, providing good conductivity and line edge definition combined with acceptable ink usage and the inks were jetted reliably and reproducibly at 30 V and 35 °C temperature, using frequent cleaning cycles during the printing. Each ink was printed at a maximum jetting frequency of 5 kHz. A few layers of inks were printed to produce a conductive pattern of 1 cm × 1 cm area at first for optimizing the electrical conductivity and then thermally cured at different times and temperatures for optimization of the electrical conductivity in an oven to sinter the conductive inks. To demonstrate the potential of electronic textiles applications of conductive inks, a conductive track at the specified area (Figure S4d,e, Supporting Information) was then inkjet-printed onto 100% Tencel fabrics by depositing optimized layers for making the textile electrodes for sensors and the resistance was measured with a digital multimeter (Keithley, DMM7510).

E-textiles' performance: By following previously reported methods[54] the flexibility of coated and inkjet-printed e-textiles was evaluate. Various cord lengths were used to measure the change of resistance of inkjet-printed (10 cm × 1 cm strip) during bending (concave down) and compression (concave upward). A Win-Test tensile tester (Testometric, UK) was used to control the cord length both in the forward and reverse directions for both bending and compression tests. The change in the electrical resistance of the textiles during bending and compressions was captured using a Keithley digital multimeter (DMM7510).

Textile electrode fabrication and performance for vital sign sensing: Wearable e-textiles for vital sign sensing require the integration of high-performance electrode materials to ensure accurate health monitoring.[55–60] The wearable textile electrode was then fabricated by fully inkjet printing with optimized layers onto surface-treated Tencel fabric and at the edges of the printed textile, electrode connecting wires were attached as current collectors. The electrical performances were investigated with a multimeter attached to the connection. For temperature sensor analysis, the printed area of electrode was 2 cm × 2 cm and for ECG studies three electrodes were used, with each electrode area being 3 cm × 1 cm.

For ECG signal and heart rate measurement with the Go Direct® EKG device, we attached one connecting wire to each electrode patch. This device measures electrical activity in the heart and electrical signals produced during muscle contractions. For this device, we used the 3-lead ECG tracings settings and attached our prepared electrode patches to the subject as shown in Figure 3a following our previous study[61] as per the guidelines.[62] The textile selected for this study is Tencel fabric, which offers properties such as softness, breathability, and flexibility. These characteristics enhance the fabric's conformity to the skin's surface, ensuring a better fit. Furthermore, the ink materials adhered to the textile closely follow the skin's contours, reducing air gaps and improving contact. This, in turn, lowers the contact resistance. Additionally, PEDOT:PSS and graphene, respectively, were chosen for their conductive properties, ensuring that the textile remains conductive even under deformation, further improving the contact stability. To maintain proper pressure between the textile electrodes and the skin, we wrapped and secured electrodes around the wrist and forearm for ECG measurement on the hand with stretchable film. A single patch was placed on the inside of the right wrist, on the inside of the right upper forearm (distal to the elbow) and on the inside of the left upper forearm (distal to elbow) and the reference device's clips were connected to the electrode tabs as shown in Figure 3a. The subject was in a relaxed position (sitting) in a chair for measurements of ECG and heart rate and the ECG channel used a low-pass filter that has been optimized for recording ECGs. This is the default channel that is active when the sensor is connected. The default active channel was optimized for recording ECGs, utilizing a low-pass filter with a 22.5 Hz −3 dB cutoff and −80 dB attenuation above 50 Hz. Simultaneously, the heart rate channel, initially inactive upon connection, detects QRS waveforms and computes the heart rate in bpm within a 6-second sampling window, updating the value every second. The heart rate channel detected QRS waveforms and used that data to calculate the heart rate in bpm. The sampling window for this calculation was 6 s and the value updated every second.

To assess the resistance dependence on temperature, a resistance measurement setup was used together with a hotplate to observe the heating and cooling cycle. In the resistance measurement setup, a digital multimeter was used, and the sensor was placed on a hotplate to drive the heating/cooling process. To prevent layer scratching, the two connecting wires to the temperature sensor electrode in the sensitivity measurement setup connection were embedded in the fabric. The sensitivity of the temperature sensor was defined by its TCR and can be calculated from Equation (2):

$$\mathrm{TCR}\ \left(\%^{\circ}\mathrm{C}^{-1}\right) = \frac{(R - R_0)}{R_0 \times \Delta T} \times 100 \quad (1)$$

where R and R_0 are the resistance at the measured temperature and room temperature of the sensor, and ΔT is the change in applied temperature.[63] Furthermore, the electrode was attached to the outside of a glass jar to confirm the hot water temperature over the electrode. Also, the textile electrode worn by the subject for measuring the sensitivity in skin surface temperature was as illustrated in Figure 3m. Thus, we measured the resistance of the electrode at skin surface temperature and room temperature (~25 °C) to calculate TCR from both type of electrodes. The printed sensor will be compared with the commercially available circuit module MAX30205.

To investigate the concurrent vital sign monitoring by the wearable e-textiles all the textile electrodes were attached inside a pair of textile gloves and data for temperature sensitivity, ECG signal processing and heart rate were measured and collated, Figure 4b and Figure S5, Supporting Information. The integration of SWEET with the gloves was achieved using double-sided adhesive tape, ensuring a

secure and stable connection between the sensor and the glove material. The data of human participant's vital sign-heart rate and resistance change due to varying temperature is given in Table S1, Supporting Information.

Soil burial testing: To assess the sensor electrode biodegradability, soil burial tests in an unglazed pot was undertaken, with 150 mm filling soil height and hole in the base for exchange of air. The test soil had a pH between 6.5 and 6.8, white and green peat, with identical water content and amounts of soil (120 g) to bury each sample in the pot. Two burial periods, 1 and 4 months, were used to investigate short-term and medium-term effects (Figure S6a,b, Supporting Information) following earlier studies,[64] where a maximum 4-month burial period was undertaken. For each fabric type, test samples were cut and subsequently weighed under standard lab conditions (20 ± 2 °C temperature and $65 \pm 4\%$ relative humidity). Fabric samples were categorized into two groups: pre-burial (control) and after burial. In each category, we had four types of fabric: (1) the untreated Tencel fabric, (2) surface treated Tencel fabric with interface layer, (3) PEDOT:PSS-, and (4) graphene inkjet-printed over surface treated Tencel fabric. The conductive track was applied as a rectangle measuring 10 cm × 1 cm, positioned centrally on a strip of fabric that was at least 15 cm long and 2 cm wide, to facilitate easy handling in subsequent processes. Two replicates were conducted for each fabric type and burial interval and the test samples were placed into pots for burial in accordance with ISO 11721-1:2001.[64,65] Two specimens for each fabric type were soil buried 50 mm apart, in a U-form, with the center portion of 150 mm in intimate contact with the soil and soil pressed lightly over the specimens.

The soil burial test lasted for 4 months, from May 2023 to August 2023, with the temperature and relative humidity in the soil regularly monitored and kept constant during the experiment by incubating the soil containers at 29 ± 1 °C, at relative humidity of $90 \pm 2\%$ (Constant climate chamber HPP, Cooled incubator IPP Plus from Germany, Memmert GmbH+Co.KG). After 1 and 4 months, the fabric samples were removed from the soil. In addition to the fabric samples, the burial soil was also collected for subsequent soil analyses (Figure S6c, Supporting Information). The fabric samples were gently rinsed under running water after being removed from the soil and were then submerged in 70/30 ethanol/water for 30 min before drying at 45 ± 5 °C. The weight and tensile strength losses were then determined, and characterization analyses were conducted. The surface morphology of the untreated fabric, surface treated fabric as well as PEDOT:PSS and graphene inkjet-printed, respectively, before and after soil burial were analyzed using a FEI Quanta 650 field emission scanning electron microscope (SEM).

Determination of weight and tensile strength loss (%) after soil burial: The test fabrics were rinsed, dried, conditioned for 24 h under standard lab conditions, and then weighed before and after soil burial. The weights of the buried and control fabrics were compared and the weight loss percentage calculated via the following formula to establish biodegradability:

$$\text{Weight loss } (\%) = \frac{W_0 - W_t}{W_0} \times 100 \quad (2)$$

where W_0 and W_t correspond to the initial weight and that after being buried in soil, respectively.

A testometric materials tensile machine, load cell 100 with a testing speed of 100 mm min^{-1}, was then used to determine the tensile strength of the buried and unburied test specimens. Prior to testing the specimen size was prepared by fraying down the buried and unburied fabrics from both sides to give a central width of 2 cm and maintaining a distance between jaws of 10 cm as the gauge length.

$$\text{Tensile strenghth loss } (\%) = \frac{F_0 - F_t}{F_0} \times 100 \quad (3)$$

where F_0 and F_t correspond to the initial force and that after being buried in soil, respectively.

Determination of the number of colonies in the soil: Soil samples were collected at day 0 (before introducing test fabrics), 1 and 4 months after fabric burial and analyzed to determine the microbial levels following BS EN ISO 6222:1999, and SM 9610 A and B:1998. A 5 g soil sample was homogenized in quarter strength Ringer's solution, and subsequently diluted and pour plated to enable determination of viable microorganisms using the following agar types. Total heterotrophic plate counts (bacteria and fungi) were enumerated on Yeast Extract Agar (Oxoid; CM0019B), total bacterial counts under low nutrient conditions were enumerated on R2A agar (Oxoid; CM0906B), and fungal enumeration was undertaken on Rose Bengal Chloramphenicol Agar (Oxoid; CM1148B and SR0078E). Viable count, in colony forming units per gram (CFU g^{-1}), was calculated using Microsoft Excel spreadsheet editor (Microsoft Office Suites 365, Microsoft Corporation) and a two-way ANOVA statistical analysis was undertaken to determine significant differences ($p \leq 0.05$) using GraphPad Prism 10 (GraphPad Prism version 10.0.0 (153), GraphPad Software LLC).

LCA methodology: According to ISO 14040 and 14044 standards and frameworks, the LCA methodology as a prospective approach was used in this case for the PEDOT:PSS and graphene inkjet-printed textile electrode of a rectangle pattern of 10 cm × 1 cm area.[46,47] Following are the steps of the LCA methodology (Supporting Information): (1) goal and scope definition, (2) inventory analysis (Table S2, Supporting Information), and (3) impact assessment (Table S3, Supporting Information).

Acknowledgements

The authors gratefully acknowledge funding from Commonwealth Scholarship Commission (CSC) U.K. for a Ph.D. scholarship for Marzia Dulal, and UKRI Research England the Expanding Excellence in England (E3) grant.

Conflict of Interest

The authors declare no competing Interests. UWE Research Ethics Committee has approved Dr Shaila Afroj to perform vital sign monitoring tests (Ref No. ACE. 21. 11. 010).

Supporting Information

Supporting Information is available from the Wiley Online Library or from the author.

Keywords

e-textiles, graphene, smart textiles, sustainability, wearable electronics

Received: August 29, 2024
Revised: October 10, 2024
Published online: November 5, 2024

[1] L. Zhang, M. Y. Leung, S. Boriskina, X. Tao, *Nat. Sustain.* **2023**, *6*, 243.
[2] *UN Helps Fashion Industry Shift to Low Carbon*. **2018**. https://unfccc.int/news/un-helps-fashion-industry-shift-to-low-carbon (accessed: September 2024).
[3] N. Karim, S. Afroj, K. Lloyd, L. C. Oaten, D. V. Andreeva, C. Carr, A. D. Farmery, I.-D. Kim, K. S. Novoselov, *ACS Nano* **2020**, *14*, 12313.
[4] K. Zhang, X. Shi, H. Jiang, K. Zeng, Z. Zhou, P. Zhai, L. Zhang, H. Peng, *Nat. Protoc.* **2024**, *19*, 1557.
[5] A. Weidenkaff, R. Wagner-Wenz, A. Veziridis, *Nat. Rev. Mater.* **2021**, *6*, 462.
[6] J.-Y. Yoo, S. Oh, W. Shalish, W.-Y. Maeng, E. Cerier, E. Jeanne, M.-K. Chung, S. Lv, Y. Wu, S. Yoo, A. Tzavelis, J. Trueb, M. Park, H. Jeong, E. Okunzuwa, S. Smilkova, G. Kim, J. Kim, G. Chung, Y. Park, A. Banks, S. Xu, G. M. Sant'Anna, D. E. Weese-Mayer, A. Bharat, J. A. Rogers, *Nat. Med.* **2023**, *29*, 3137.
[7] R. Y. Tay, Y. Song, D. R. Yao, W. Gao, *Mater. Today* **2023**, *71*, 135.
[8] J. Shi, S. Liu, L. Zhang, B. Yang, L. Shu, Y. Yang, M. Ren, Y. Wang, J. Chen, W. Chen, Y. Chai, X. Tao, *Adv. Mater.* **2020**, *32*, 1901958.

[9] G. Chen, X. Xiao, X. Zhao, T. Tat, M. Bick, J. Chen, *Chem. Rev.* **2021**, *122*, 3259.
[10] M. Shahabuddin, M. N. Uddin, J. I. Chowdhury, S. F. Ahmed, M. N. Uddin, M. Mofijur, M. A. Uddin, *Int. J. Environ. Sci. Technol.* **2023**, *20*, 4513.
[11] S. Dey, G. Veerendra, S. S. A. B. Padavala, A. P. Manoj, *Green Anal. Chem.* **2023**, *7*, 100085.
[12] A. R. Köhler, L. M. Hilty, C. Bakker, *J. Ind. Ecol.* **2011**, *15*, 496.
[13] M. Ribul, A. Lanot, C. Tommencioni Pisapia, P. Purnell, S. J. McQueen-Mason, S. Baurley, *J. Clean. Prod.* **2021**, *326*, 129325.
[14] W. Wang, Y. Pan, Y. Shui, T. Hasan, I. M. Lei, S. G. S. Ka, T. Savin, S. Velasco-Bosom, Y. Cao, S. B. P. McLaren, Y. Cao, F. Xiong, G. G. Malliaras, Y. Y. S. Huang, *Nat. Electron.* **2024**, *7*, 586.
[15] M. Galliani, L. M. Ferrari, G. Bouet, D. Eglin, E. Ismailova, *APL Bioeng.* **2023**, *7*, 016101.
[16] Z. Li, V. Ruiz, V. Mishukova, Q. Wan, H. Liu, H. Xue, Y. Gao, G. Cao, Y. Li, X. Zhuang, *Adv. Funct. Mater.* **2022**, *32*, 2108773.
[17] S. C. Shen, E. Khare, N. A. Lee, M. K. Saad, D. L. Kaplan, M. J. Buehler, *Chem. Rev.* **2023**, *123*, 2242.
[18] H. H. Shi, Y. Pan, L. Xu, X. Feng, W. Wang, P. Potluri, L. Hu, T. Hasan, Y. Y. S. Huang, *Nat. Mater.* **2023**, *22*, 1294.
[19] K. Zeng, X. Shi, C. Tang, T. Liu, H. Peng, *Nat. Rev. Mater.* **2023**, *8*, 552.
[20] N. Karim, S. Afroj, A. Malandraki, S. Butterworth, C. Beach, M. Rigout, K. S. Novoselov, A. J. Casson, S. G. Yeates, *J. Mater. Chem. C* **2017**, *5*, 11640.
[21] B. A. Kuzubasoglu, E. Sayar, S. K. Bahadir, *IEEE Sensors J.* **2021**, *21*, 13090.
[22] E. Bihar, T. Roberts, E. Ismailova, M. Saadaoui, M. Isik, A. Sanchez-Sanchez, D. Mecerreyes, T. Hervé, J. B. De Graaf, G. G. Malliaras, *Adv. Mater. Technol.* **2017**, *2*, 1600251.
[23] M. Y. Teo, K. Lim, K. C. Aw, S. Kee, J. Stringer, *RSC Adv.* **2023**, *13*, 26267.
[24] N. Karim, S. Afroj, S. Tan, K. S. Novoselov, S. G. Yeates, *Sci. Rep.* **2019**, *9*, 8035.
[25] Y. Khan, A. E. Ostfeld, C. M. Lochner, A. Pierre, A. C. Arias, *Adv. Mater.* **2016**, *28*, 4373.
[26] R. F. Fonkou, M. A. Savi, *Fractal Fract.* **2023**, *7*, 592.
[27] S. Mehta, N. Lingayat, S. Sanghvi, *Expert. Syst.* **2009**, *26*, 125.
[28] A. Spanu, A. Mascia, G. Baldazzi, B. Fenech-Salerno, F. Torrisi, G. Viola, A. Bonfiglio, P. Cosseddu, D. Pani, *Front. Bioeng. Biotechnol.* **2022**, *10*, 820217.
[29] M. Alizadeh-Meghrazi, B. Ying, A. Schlums, E. Lam, L. Eskandarian, F. Abbas, G. Sidhu, A. Mahnam, B. Moineau, M. R. Popovic, *Biomed. Eng.* **2021**, *20*, 68.
[30] K. Lim, H. Seo, W. G. Chung, H. Song, M. Oh, S. Y. Ryu, Y. Kim, J.-U. Park, *Commun. Mater.* **2024**, *5*, 49.
[31] J. Kim, M. Lee, H. J. Shim, R. Ghaffari, H. R. Cho, D. Son, Y. H. Jung, M. Soh, C. Choi, S. Jung, *Nat. Commun.* **2014**, *5*, 5747.
[32] A. M. Nardes, R. A. Janssen, M. Kemerink, *Adv. Funct. Mater.* **2008**, *18*, 865.
[33] A. A. Balandin, S. Ghosh, W. Bao, I. Calizo, D. Teweldebrhan, F. Miao, C. N. Lau, *Nano Lett.* **2008**, *8*, 902.
[34] T. Q. Trung, N. T. Tien, D. Kim, J. H. Jung, O. J. Yoon, N. E. Lee, *Adv. Mater.* **2012**, *24*, 5254.
[35] J. Min, S. Demchyshyn, J. R. Sempionatto, Y. Song, B. Hailegnaw, C. Xu, Y. Yang, S. Solomon, C. Putz, L. E. Lehner, J. F. Schwarz, C. Schwarzinger, M. C. Scharber, E. Shirzaei Sani, M. Kaltenbrunner, W. Gao, *Nat. Electron.* **2023**, *6*, 630.
[36] J. Tu, J. Min, Y. Song, C. Xu, J. Li, J. Moore, J. Hanson, E. Hu, T. Parimon, T.-Y. Wang, E. Davoodi, T. F. Chou, P. Chen, J. J. Hsu, H. B. Rossiter, W. Gao, *Nat. Biomed. Eng.* **2023**, *7*, 1293.
[37] J. R. Walter, S. Xu, J. A. Rogers, *Nat. Commun.* **2024**, *15*, 123.
[38] M. R. Islam, S. Afroj, N. Karim, *ACS Nano* **2023**, *17*, 18481.
[39] I. Ali, M. R. Islam, J. Yin, S. J. Eichhorn, J. Chen, N. Karim, S. Afroj, *ACS Nano* **2024**, *18*, 3871.
[40] J. Kim, S. Yoo, C. Liu, S. S. Kwak, J. R. Walter, S. Xu, J. A. Rogers, *Nat. Rev. Bioeng.* **2023**, *1*, 631.
[41] S. Bhattacharjee, R. Joshi, A. A. Chughtai, C. R. Macintyre, *Adv. Mater. Interfaces* **2019**, *6*, 1900622.
[42] S. Khan, M. Naushad, E. C. Lima, S. Zhang, S. M. Shaheen, J. Rinklebe, *J. Hazard. Mater.* **2021**, *417*, 126039.
[43] K. Arshad, M. Skrifvars, V. Vivod, J. V. Valh, B. Vončina, *Tekstilec* **2014**, *57*, 118.
[44] Y. Plekhanova, S. Tarasov, A. Reshetilov, *Biosensors* **2021**, *11*, 332.
[45] G. Wernet, S. Conradt, H. P. Isenring, C. Jiménez-González, K. Hungerbühler, *Int. J. Life Cycle Assess.* **2010**, *15*, 294.
[46] International Organization for Standardization, Environmental management: life cycle assessment; Principles and Framework. ISO **2006**.
[47] M. Finkbeiner, *Int. J. Life Cycle Assess.* **2014**, *19*, 266.
[48] L. B. Azevedo, R. van Zelm, P. M. Elshout, A. J. Hendriks, R. S. Leuven, J. Struijs, D. de Zwart, M. A. Huijbregts, *Glob. Ecol. Biogeogr.* **2013**, *22*, 1304.
[49] S. Sarma Choudhury, N. Katiyar, R. Saha, S. Bhattacharya, *Sci. Rep.* **2024**, *14*, 1597.
[50] M. R. Islam, S. Afroj, J. Yin, K. S. Novoselov, J. Chen, N. Karim, *Adv. Sci.* **2023**, *11*, 2304140.
[51] I. Ali, N. Karim, S. Afroj, *EcoMat* **2024**, *6*, e12471.
[52] D. McManus, S. Vranic, F. Withers, V. Sanchez-Romaguera, M. Macucci, H. Yang, R. Sorrentino, K. Parvez, S.-K. Son, G. Iannaccone, K. Kostarelos, G. Fiori, C. Casiraghi, *Nat. Nanotechnol.* **2017**, *12*, 343.
[53] M. R. Islam, S. Afroj, K. S. Novoselov, N. Karim, *Adv. Funct. Mater.* **2024**, DOI: 10.1002/adfm.202410666.
[54] M. R. Islam, S. Afroj, C. Beach, M. Islam, C. Parraman, A. Abdelkader, A. Casson, K. Novoselov, N. Karim, *iScience* **2022**, *25*, 103945.
[55] M. Zhang, Y. Yang, H. Hu, S. Zhao, W. Song, N. Karim, H. Hu, *ACS Appl. Mater. Interfaces* **2024**, *16*, 49845.
[56] I. Ali, M. Dulal, N. Karim, S. Afroj, *Small Struct.* **2024**, *5*, 2300282.
[57] S. Afroj, L. Britnell, T. Hasan, D. V. Andreeva, K. S. Novoselov, N. Karim, *Adv. Funct. Mater.* **2021**, *31*, 2107407.
[58] S. Tan, M. R. Islam, H. Li, A. Fernando, S. Afroj, N. Karim, *Adv. Sensor Res.* **2022**, *1*, 2200010.
[59] S. Tan, S. Afroj, D. Li, M. R. Islam, J. Wu, G. Cai, N. Karim, Z. Zhao, *iScience* **2023**, *26*, 106403.
[60] S. Afroj, M. H. Islam, N. Karim, *Proceedings* **2021**, *68*, 11.
[61] M. Dulal, S. Afroj, M. R. Islam, M. Zhang, Y. Yang, H. Hu, K. S. Novoselov, N. Karim, *Small* **2024**, DOI: 10.1002/smll.202407207.
[62] *Go Direct® EKG Sensor User Manual*, https://www.vernier.com/manuals/gdx-ekg/ (accessed: September 2023).
[63] Y.-F. Wang, T. Sekine, Y. Takeda, K. Yokosawa, H. Matsui, D. Kumaki, T. Shiba, T. Nishikawa, S. Tokito, *Sci. Rep.* **2020**, *10*, 2467.
[64] V. Sular, G. Devrim, *Fibres Text. East. Eur.* **2019**, *27*, 100.
[65] D. Klemenčič, B. Simončič, B. Tomšič, B. Orel, *Carbohydr. Polym.* **2010**, *80*, 426.